LUND UNIVERSITY

Inverse scattering for anisotropic mirror image invariant media

Friden, Jonas

1993

[Link to publication](#)

Total number of authors:
1

Inverse Scattering for Anisotropic Mirror Image Invariant Media

Jonas Fridén

Electromagnetic Theory
Department of Electrical and Information Technology
Lund University
Sweden

Jonas Fridén

Institute of Theoretical Physics
Chalmers University of Technology
University of Göteborg
SE-412 96 Göteborg
Sweden

Abstract

Basic tools to solve an inverse scattering problem for anisotropic media are developed. A transient electromagnetic field impinges upon a slab of anisotropic dispersive medium. The scattering kernels map the incident field to the scattered fields. The inverse scattering problem is to reconstruct the components of the matrix susceptibility kernel from knowledge of the scattering kernels. The method is based on the imbedding and Green functions equations. These equations are generalized to allow for an incident field at arbitrary angle from one side of the slab and the mirror image field incident from the other side of the slab. Mirror image invariance is investigated for a homogeneous slab. An inverse scattering problem for a homogeneous mirror image invariant medium is presented and solved numerically using reflection data from one side of the slab only.

1 Introduction

Electromagnetic wave propagation and scattering problems in stratified anisotropic media have been treated by many authors in the last decades. For some fundamental developments in the optical regime see, e.g. Refs [2, 19, 22]. More recent developments may be found in, e.g. Refs [6, 7, 20, 23, 25]. There is also some work carried out for inhomogeneous media at fixed frequency [10, 17]. However, in recent years there has been an intensified interest in studying scattering problems using time-domain techniques. In Ref. [21] both the direct and the inverse scattering problem for a stratified dielectric (non-dispersive) anisotropic slab were discussed and in Ref. [8] the direct scattering problem for the stratified dispersive anisotropic slab was solved. The objective of this paper is to establish the basic tools to solve an inverse scattering problem for a slab of dispersive anisotropic medium using time-domain techniques.

The scattering problem is that of an incident electromagnetic plane wave impinging obliquely on an anisotropic, source-free, dispersive, stratified slab of finite or infinite thickness. Outside the slab there is vacuum and, furthermore, there are no phase velocity mismatches at the boundaries of the slab. The incident field gives rise to a reflected and a transmitted field. Now, if the electromagnetic properties of the slab are known, the scattered fields can be calculated. This is the direct scattering problem and it was addressed and solved in Ref. [8]. The inverse scattering problem is the reverse problem, i.e., to reconstruct the electromagnetic properties of the slab from scattering data.

The electromagnetic properties of the slab are represented by a 3×3 dyadic susceptibility kernel $\overline{\overline{\chi}}$. Hence, the medium is characterized by 9 scalar susceptibility kernels in the most general case. In a cartesian coordinatesystem with z-axis normal to the planes of stratification and to the boundaries of the slab and y-axis in the plane of the incident wave, the susceptibility dyadic kernel is represented by the 3×3 matrix

$$\boldsymbol{\chi}(z,t) = \begin{pmatrix} \chi_{11} & \chi_{12} & \chi_{13} \\ \chi_{21} & \chi_{22} & \chi_{23} \\ \chi_{31} & \chi_{32} & \chi_{33} \end{pmatrix}(z,t)$$

The generic output of the direct scattering problem, and the input of the inverse scattering problem, is the scattering kernels. These kernels map the incident field to the scattered, reflected and transmitted fields, respectively. The main objective of this study is therefore to develop equations that relate the scattering kernels to the susceptibility kernels in such a way that the inverse problem can be solved. To do this a wave splitting technique is used (see Refs [1, 5, 8, 14, 24]). In vacuum the wave splitting is a decomposition of the electromagnetic field into its right- and left-moving parts. The split fields are used in an imbedding method, first used in Ref. [1], and a Green functions method (see Ref. [11]). These methods have been used and further developed in Refs [5, 13, 14, 18].

In this study the imbedding and Green functions methods are generalized to allow for incident fields from both sides of the slab. Specifically, a scattering experiment and its mirror image are studied. These two experiments complement each other in the solution of the general inverse scattering problem (to be addressed in a subsequent paper). However, there are media (mirror image invariant) where scattering data from mirror image scattering experiments are just the mirror images of each other. For homogeneous media and arbitrary angle of incidence, the slab is mirror image invariant if

$$\boldsymbol{\chi}(t) = \begin{pmatrix} \chi_{11} & \chi_{12} & 0 \\ \chi_{21} & \chi_{22} & 0 \\ 0 & 0 & \chi_{33} \end{pmatrix}(t)$$

Such media are treated in, e.g. Refs [16, 20].

To reconstruct the five susceptibility kernels of a mirror image invariant medium an algorithm using only reflection data from one side of the slab has been constructed. This algorithm uses reflection data from one experiment at normal incidence and one at oblique incidence (for simplicity the angle $\frac{\pi}{3}$ has been chosen). Synthetic direct scattering data are calculated with the Green functions method and the inverse algorithm uses the imbedding equation for the reflection kernel. In this way any bias to a specific method in solving the inverse scattering problem is avoided. Finally, some illustrating numerical examples are presented in Section 9.

Dyadics ($\overline{\overline{b}}$) and vectors ($\boldsymbol{b}$ or a unit-vector $\hat{b}$) are displayed italic. Matrices (**b**) are displayed roman boldface. The symbol $*$ is a shorthand notation for convolution. If a dyadic is convolved with a vector an additional scalar product is understood. For example

$$\overline{\overline{\chi}}(\boldsymbol{r},\cdot) * \boldsymbol{E}(\boldsymbol{r},\cdot)(t) = \int_{-\infty}^{t} \overline{\overline{\chi}}(\boldsymbol{r}, t-t') \cdot \boldsymbol{E}(\boldsymbol{r},t')dt'$$

A $*$-product of matrices denotes an additional ordinary matrix product etc. Both the notation (x,y,z) and $(1,2,3)$ are used to label the axes of a right-handed cartesian coordinate system throughout the paper.
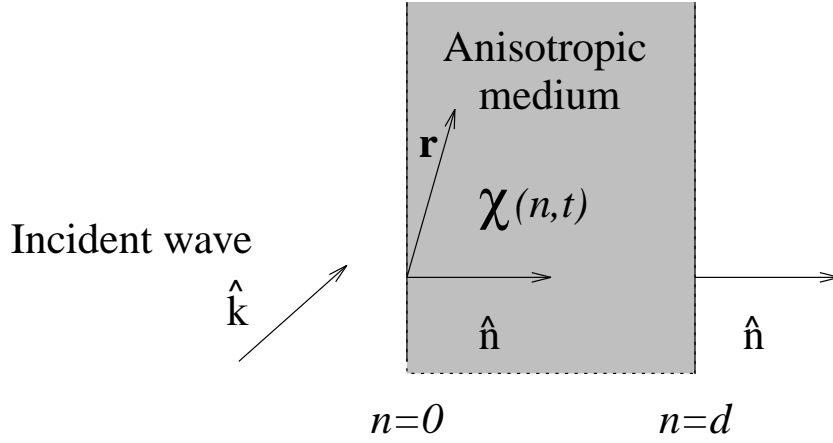
Figure 1: The geometry of the scattering problem.

2 Coordinate system independent equations

To investigate the inverse scattering problem for an anisotropic slab, and to study its underlying symmetries, it is advantageous to formulate the field equations in a coordinate system independent form. This is performed by introducing a dyadic notation. Consider an incident plane wave along $\hat{k}$ and an anisotropic slab with stratification along $\hat{n}$ (see Fig. 1). The Maxwell equations, in a source-free region, are

$$\begin{cases} \nabla \times \boldsymbol{E}(\boldsymbol{r},t) = -\dfrac{\partial \boldsymbol{B}(\boldsymbol{r},t)}{\partial t} \\ \nabla \times \boldsymbol{H}(\boldsymbol{r},t) = \dfrac{\partial \boldsymbol{D}(\boldsymbol{r},t)}{\partial t} \end{cases}$$

The following constitutive relations with time convolutions are adopted (see Refs [8,9])

$$\begin{cases} \boldsymbol{D}(\boldsymbol{r},t) = \epsilon_0 \left(\boldsymbol{E}(\boldsymbol{r},t) + \overline{\overline{\chi}}(\boldsymbol{r},\cdot) * \boldsymbol{E}(\boldsymbol{r},\cdot)(t) \right) \\ \boldsymbol{B}(\boldsymbol{r},t) = \mu_0 \boldsymbol{H}(\boldsymbol{r},t) \end{cases}$$

where ϵ_0, μ_0 are the permittivity and permeability of vacuum, respectively. The phase velocity, c_0 and the wave impedance η_0 of vacuum are

$$c_0 = \frac{1}{\sqrt{\epsilon_0\mu_0}} \qquad \eta_0 = \sqrt{\frac{\mu_0}{\epsilon_0}}$$

The dispersive properties of the medium are modelled by the 3×3 susceptibility dyadic $\overline{\overline{\chi}}$.

All vectors are decomposed in components normal and parallel to the planes of stratification (normal vector $\hat{n}$).

$$\hat{k} = \boldsymbol{k}_\parallel + k_n \hat{n}$$
$$\boldsymbol{E} = \boldsymbol{E}_\parallel + E_n \hat{n}$$
$$\boldsymbol{H} = \boldsymbol{H}_\parallel + H_n \hat{n}$$

The dyadic $\overline{\overline{\chi}}$ is decomposed in a similar fashion [15]

$$\overline{\overline{\chi}} = \overline{\overline{\chi}}_\parallel + \hat{n}\boldsymbol{a} + \boldsymbol{b}\hat{n} + \hat{n}c\hat{n} \tag{2.1}$$

where the dyadic $\overline{\overline{\chi}}_\parallel$ and the vectors $\boldsymbol{a}$ and $\boldsymbol{b}$ are perpendicular to $\hat{n}$ and c is a scalar, do not confuse with c_0. The explicit forms are obtained from the decomposition of the unit dyadic $\overline{\overline{I}} = -(\hat{n} \times \overline{\overline{I}})(\hat{n} \times \overline{\overline{I}}) + \hat{n}\hat{n}$

$$\overline{\overline{\chi}}_\parallel = (\hat{n} \times \overline{\overline{I}})[(\hat{n} \times \overline{\overline{I}})\overline{\overline{\chi}}(\overline{\overline{I}} \times \hat{n})](\overline{\overline{I}} \times \hat{n})$$
$$\boldsymbol{a} = -[\hat{n} \cdot \overline{\overline{\chi}}(\overline{\overline{I}} \times \hat{n})](\overline{\overline{I}} \times \hat{n}) \tag{2.2}$$
$$\boldsymbol{b} = -(\hat{n} \times \overline{\overline{I}})[(\hat{n} \times \overline{\overline{I}})\overline{\overline{\chi}} \cdot \hat{n}]$$
$$c = \hat{n} \cdot \overline{\overline{\chi}} \cdot \hat{n}$$

Due to the stratification of the slab and the plane wave form of the incoming wave, the fields can be written as

$$\boldsymbol{E}(\boldsymbol{r}, t) = \boldsymbol{E}(\boldsymbol{r} \cdot \hat{n}, t - \frac{\boldsymbol{r} \cdot \boldsymbol{k}_\parallel}{c_0})$$
$$\boldsymbol{H}(\boldsymbol{r}, t) = \boldsymbol{H}(\boldsymbol{r} \cdot \hat{n}, t - \frac{\boldsymbol{r} \cdot \boldsymbol{k}_\parallel}{c_0})$$

This implies that the fields at $(\boldsymbol{r}, t)$ are identical to the fields at an earlier time $t - \frac{\boldsymbol{r} \cdot \boldsymbol{k}_\parallel}{c_0}$ at the point $(\boldsymbol{r} \cdot \hat{n})\hat{n}$. Hence, two independent coordinates

$$n = \boldsymbol{r} \cdot \hat{n} \qquad s = t - \frac{\boldsymbol{r} \cdot \boldsymbol{k}_\parallel}{c_0}$$

are introduced.

The problem can be formulated with the parallel fields only. In order to eliminate the normal components of the fields, study the normal components of the Maxwell equations. An integration with respect to s yields

$$\begin{cases} \boldsymbol{0} = \boldsymbol{k}_\parallel \times \boldsymbol{E}_\parallel - \eta_0 H_n \hat{n} \\ \boldsymbol{0} = \boldsymbol{k}_\parallel \times \eta_0 \boldsymbol{H}_\parallel + \hat{n}E_n + \hat{n}\boldsymbol{a} * \boldsymbol{E}_\parallel + c * E_n \hat{n} \end{cases} \tag{2.3}$$

The first equation gives $H_n(n, s)$ directly and the second can be solved for $E_n(n, s)$ since it is a Volterra equation of the second kind in E_n. Hence, for each c there is a resolvent L such that

$$\begin{cases} c + L + c * L = 0 \\ E_n = (1 + L*)\left[\boldsymbol{k}_\parallel \cdot (\hat{n} \times \eta_0 \boldsymbol{H}_\parallel) - \boldsymbol{a} * \boldsymbol{E}_\parallel\right] \end{cases} \tag{2.4}$$

In the parallel components of the Maxwell equations both parallel and normal components of the fields appear. Elimination of the normal field-components gives the following PDE for the parallel field-components

$$
\begin{aligned}
c_0 \partial_n \begin{pmatrix} \boldsymbol{E}_\parallel \\ \hat{n} \times \eta_0 \boldsymbol{H}_\parallel \end{pmatrix} = & \begin{pmatrix} \overline{\overline{0}} & \overline{\overline{I}}_2 - \boldsymbol{k}_\parallel \boldsymbol{k}_\parallel \\ \overline{\overline{I}}_2 - (\boldsymbol{k}_\parallel \times \hat{n})(\boldsymbol{k}_\parallel \times \hat{n}) & \overline{\overline{0}} \end{pmatrix} \partial_s \begin{pmatrix} \boldsymbol{E}_\parallel \\ \hat{n} \times \eta_0 \boldsymbol{H}_\parallel \end{pmatrix} \\
& + \begin{pmatrix} \overline{\overline{D}}_{ee} & -\overline{\overline{D}}_{em} \\ \overline{\overline{D}}_{me} & \overline{\overline{D}}_{mm} \end{pmatrix} * \partial_s \begin{pmatrix} \boldsymbol{E}_\parallel \\ \hat{n} \times \eta_0 \boldsymbol{H}_\parallel \end{pmatrix}
\end{aligned}
\tag{2.5}
$$

where

$$
\begin{aligned}
\overline{\overline{D}}_{ee} &= \boldsymbol{k}_\parallel (1 + L*) \boldsymbol{a} \\
\overline{\overline{D}}_{em} &= \boldsymbol{k}_\parallel L \boldsymbol{k}_\parallel \\
\overline{\overline{D}}_{me} &= \overline{\overline{\chi}}_\parallel - \boldsymbol{b} * (1 + L*) \boldsymbol{a} \\
\overline{\overline{D}}_{mm} &= \boldsymbol{b}(1 + *L) \boldsymbol{k}_\parallel
\end{aligned}
$$

The dyadic $\overline{\overline{I}}_2 = \overline{\overline{I}} - \hat{n}\hat{n}$ is the 2×2 unit dyadic perpendicular to $\hat{n}$. The first term, on the right hand side in the above PDE, comes from the vacuum part of the constitutive relations and the second one is due to the dispersion part.

3   Wave splitting

The wave splitting transformation, introduced in this section, is a transformation of the dependent variables and it makes the pricipal part of (2.5) diagonal (cf. Ref. [24]). In this case the wave splitting transformation is

$$
\begin{pmatrix} \boldsymbol{E}^+ \\ \boldsymbol{E}^- \end{pmatrix} = \overline{\overline{P}} \begin{pmatrix} \boldsymbol{E}_\parallel \\ \hat{n} \times \eta_0 \boldsymbol{H}_\parallel \end{pmatrix}
$$

where (cf. Ref. [8])

$$
\overline{\overline{P}} = \frac{1}{2} \begin{pmatrix} \overline{\overline{I}}_2 & -\overline{\overline{\Gamma}} \\ \overline{\overline{I}}_2 & \overline{\overline{\Gamma}} \end{pmatrix} \qquad \overline{\overline{P}}^{-1} = \begin{pmatrix} \overline{\overline{I}}_2 & \overline{\overline{I}}_2 \\ -\overline{\overline{\Gamma}}^{-1} & \overline{\overline{\Gamma}}^{-1} \end{pmatrix}
$$

and

$$
\overline{\overline{\Gamma}} = \frac{\overline{\overline{I}}_2 - \boldsymbol{k}_\parallel \boldsymbol{k}_\parallel}{|k_n|} \qquad \overline{\overline{\Gamma}}^{-1} = \frac{\overline{\overline{I}}_2 - (\boldsymbol{k}_\parallel \times \hat{n})(\boldsymbol{k}_\parallel \times \hat{n})}{|k_n|}
$$

This transformation implies that the PDE (2.5) transforms into

$$v\partial_n \begin{pmatrix} \boldsymbol{E}^+ \\ \boldsymbol{E}^- \end{pmatrix} = \left[\begin{pmatrix} -\overline{\overline{I}}_2 & 0 \\ 0 & \overline{\overline{I}}_2 \end{pmatrix} + \begin{pmatrix} \overline{\overline{\Delta}}_{11} & \overline{\overline{\Delta}}_{12} \\ \overline{\overline{\Delta}}_{21} & \overline{\overline{\Delta}}_{22} \end{pmatrix} * \right] \partial_s \begin{pmatrix} \boldsymbol{E}^+ \\ \boldsymbol{E}^- \end{pmatrix} \qquad (3.1)$$

The phase velocity, of the fields, along $\hat{n}$ is $v = \frac{c_0}{|k_n|}$. The $\overline{\overline{\Delta}}$ dyadics are given by

$$\begin{pmatrix} \overline{\overline{\Delta}}_{11} \\ -\overline{\overline{\Delta}}_{12} \\ \overline{\overline{\Delta}}_{21} \\ \overline{\overline{\Delta}}_{22} \end{pmatrix} = \begin{pmatrix} -1 & 1 & 1 & 1 \\ 1 & -1 & 1 & 1 \\ 1 & 1 & -1 & 1 \\ 1 & 1 & 1 & -1 \end{pmatrix} \begin{pmatrix} \overline{\overline{\Delta}}_{me} \\ \overline{\overline{\Delta}}_{ee} \\ \overline{\overline{\Delta}}_{mm} \\ \overline{\overline{\Delta}}_{em} \end{pmatrix} \qquad (3.2)$$

where

$$\begin{aligned} \overline{\overline{\Delta}}_{me} &= \frac{1}{2|k_n|} \overline{\overline{\Gamma}} \left[\overline{\overline{\chi}}_\| - \boldsymbol{b} * (1 + L*)\boldsymbol{a} \right] \\ \overline{\overline{\Delta}}_{ee} &= \frac{1}{2|k_n|} \boldsymbol{k}_\| (1 + L*)\boldsymbol{a} \\ \overline{\overline{\Delta}}_{mm} &= \frac{1}{2|k_n|^2} \overline{\overline{\Gamma}} \boldsymbol{b} (1 + *L) \boldsymbol{k}_\| \\ \overline{\overline{\Delta}}_{em} &= \frac{\boldsymbol{k}_\| \boldsymbol{k}_\|}{2|k_n|^2} L \end{aligned} \qquad (3.3)$$

The Equation (3.1) has certain analogy to the 4×4 matrix approach for fixed frequency [2, 17]. In the absence of a slab all the $\overline{\overline{\Delta}}$ dyadics vanish identically and $\boldsymbol{E}^\pm$ become fields moving in the $\pm\hat{n}$-directions, respectively. Note that $\boldsymbol{E}^\pm$ are transverse electromagnetic fields and not pure electric fields as the notation suggests. However, the sum of $\boldsymbol{E}^+$ and $\boldsymbol{E}^-$ is always the total transverse electric field. The total $\boldsymbol{E}$- and $\boldsymbol{H}$-fields may be calculated by use of (2.3) and (2.4), which give the normal components of these fields.

4 Mirror image scattering problems

The equations derived in the previous section do not depend on the sign of the normal component, k_n, of $\hat{k}$. Only the parallel component $\boldsymbol{k}_\|$ and the absolute value of the normal component $|k_n|$ enter. Hence, the equations describe two scattering experiments with incident fields along

$$\hat{k}^\pm = \boldsymbol{k}_\| \pm |k_n|\hat{n}$$

respectively. Ignoring the slab, the scattering experiments are mirror images of each other, see Fig. 2. Both experiments are useful in the solution of the inverse scattering problem for the general homogeneous medium (reconstruction of 9 functions). This problem will be addressed in a subsequent paper. To see the underlying symmetries of the scattering problem, scattering from both sides of the slab are considered in the following.
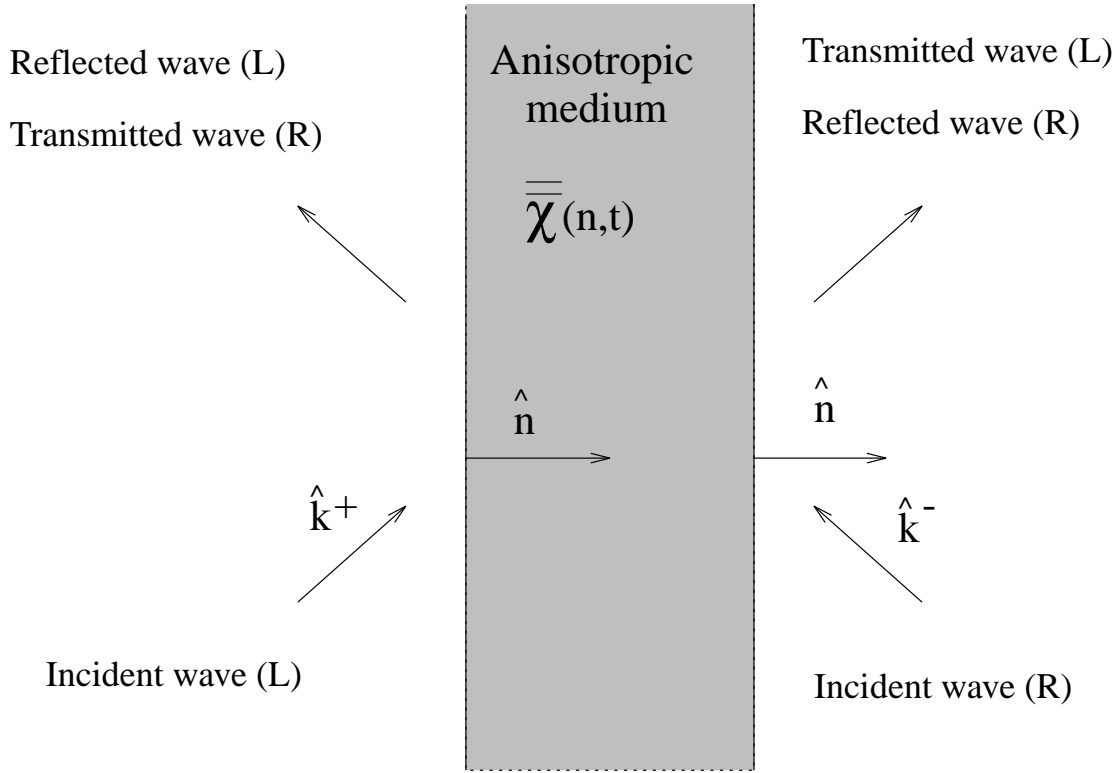
Figure 2: The geometry of the mirror image scattering experiments with incident fields along $\hat{k}^{\pm}$. The scattering experiments are labeled L and R for left and right respectively.

A fixed right-handed cartesian coordinate system with z-axis along $\hat{n}$ and y-axis in the plane of incidence is introduced. The slab of the anisotropic medium extends from $z = 0$ to $z = d$. The explicit coordinate representation of the susceptibility dyadic is

$$\overline{\overline{\chi}}_{\parallel} = \hat{x}\chi_{11}\hat{x} + \hat{x}\chi_{12}\hat{y} + \hat{y}\chi_{21}\hat{x} + \hat{y}\chi_{22}\hat{y}$$
$$\boldsymbol{a} = \chi_{31}\hat{x} + \chi_{32}\hat{y}$$
$$\boldsymbol{b} = \hat{x}\chi_{13} + \hat{y}\chi_{23}$$
$$c = \chi_{33}$$

which yields the following matrix representations, see also Ref. [8],

$$\boldsymbol{\Delta}_{me} = \frac{1}{2\cos\theta}\boldsymbol{\Gamma}\left[\boldsymbol{\chi}_{\parallel} - \begin{pmatrix} \chi_{13}*(1+L*)\chi_{31} & \chi_{13}*(1+L*)\chi_{32} \\ \chi_{23}*(1+L*)\chi_{31} & \chi_{23}*(1+L*)\chi_{32} \end{pmatrix}\right]$$

$$\boldsymbol{\Delta}_{ee} = \frac{\tan\theta}{2\cos\theta}\boldsymbol{\Gamma}(1+L*)\begin{pmatrix} 0 & 0 \\ \chi_{31} & \chi_{32} \end{pmatrix}$$

$$\boldsymbol{\Delta}_{mm} = \frac{\tan\theta}{2\cos\theta}\boldsymbol{\Gamma}(1+L*)\begin{pmatrix} 0 & \chi_{13} \\ 0 & \chi_{23} \end{pmatrix}$$

$$\boldsymbol{\Delta}_{em} = \frac{\tan^2\theta}{2\cos\theta}\boldsymbol{\Gamma}\begin{pmatrix} 0 & 0 \\ 0 & L \end{pmatrix}$$

$$\boldsymbol{\Gamma} = \begin{pmatrix} \frac{1}{\cos\theta} & 0 \\ 0 & \cos\theta \end{pmatrix}$$

The incident waves propagate along $\hat{k}^{\pm} = \sin\theta\hat{y} \pm \cos\theta\hat{z}$. Note that the representation of the dispersive properties of the slab is the same for an incident field along $\hat{k}^+$ or $\hat{k}^-$.

5 Wave fronts

The underlying PDE (3.1) for the fields $\boldsymbol{E}^{\pm}$, is hyperbolic and supports singular solutions. Any finite jump discontinuity in $\boldsymbol{E}^{\pm}$ propagates along the characteristics $s \mp z/v = \xi_{\pm}$, respectively. These discontinuities, or wave fronts, are treated by introducing wave front matrices $\boldsymbol{Q}^{\pm}$. An extensive investigation of these matrices may be found in Ref. [8]. The basic relations are

$$\left[\boldsymbol{E}^{\pm}(z_2, \xi_{\pm} + z_2/v)\right]_{-}^{+} = \mathbf{Q}^{\pm}(z_1, z_2)\left[\boldsymbol{E}^{\pm}(z_1, \xi_{\pm} + z_1/v)\right]_{-}^{+} \tag{5.1}$$

where $[\ ]_{-}^{+}$ denotes a jump discontinuity with respect to the second argument, e.g. the wave front matrix $\mathbf{Q}^{+}(z_1, z_2)$ propagates a finite jump discontinuity in $\boldsymbol{E}^{+}$ from the spatial coordinate z_1 to z_2 with speed v. The wave front matrices are determined by the medium in the slab and explicitly they are

$$\mathbf{Q}^{\pm}(z_1, z_2) = \mathcal{S}\exp\left(-\int_{\ddagger\infty}^{\ddagger\in} \mathbf{a}^{\pm}(\ddagger')\lceil\ddagger'\right)$$

where

$$\mathbf{a}^{+}(z) = -\frac{1}{v}\boldsymbol{\Delta}_{11}(z, 0^+)$$

$$\mathbf{a}^{-}(z) = -\frac{1}{v}\boldsymbol{\Delta}_{22}(z, 0^+)$$

and $\mathcal{S}$ is a spatial ordering operator (see Ref. [8]).

6   Scattering operators

For a given medium the generic output of a scattering problem is the reflection and transmission kernels. These kernels are independent of the excitation and depend only on the properties of the medium. Equations to calculate these kernels are constructed in this section. From these equations both the direct problem and the inverse problem may be solved. Two ways of computing the scattering kernels are employed; the imbedding and Green functions methods, see Ref. [8]. These methods are now further generalized to include incident fields from both sides of the slab, corresponding to incident fields along $\hat{k}^{\pm}$. This generalization is crucial for the solution of the inverse scattering problem for the general anisotropic medium. For comparison, both mirror image scattering problems are treated simultaneously. Scattering kernels corresponding to an incoming wave along $\hat{k}^{+}$ are labeled L (for left) and for an incoming wave along $\hat{k}^{-}$ the index R (for right) is used. For a detailed investigation of these equations in the case of scattering from the left see Ref. [8].

6.1   The imbedding method

The imbedding method uses the idea of studying a one parameter family of related problems. Each problem corresponds to a subsection of the physical slab $[0, d]$. For scattering from the left, the subsection is $[z, d]$, and for scattering from the right $[0, z]$ is used. As the parameter z varies from one endpoint to the other the scattering problem varies from a trivial one, where no slab is present, to the full scattering problem. This technique has been implemented in various applications during the last decade (see Refs $[1, 4, 5, 8, 14, 21]$). The scattering operators for the subslabs, with kernels $\mathbf{R}_{L,R}$ and $\mathbf{T}_{L,R}$, are defined as

$$
\begin{aligned}
&\boldsymbol{E}^{-}(z, s) = \mathbf{R}_L(z, \cdot) * \boldsymbol{E}^{+}(z, \cdot)(s) \\
&\boldsymbol{E}^{+}(d, s + (d - z)/v) = \mathbf{Q}^{+}(z, d) \left\{ \boldsymbol{E}^{+}(z, s) + \mathbf{T}_L(z, \cdot) * \boldsymbol{E}^{+}(z, \cdot)(s) \right\} \\
&\boldsymbol{E}^{+}(z, s) = \mathbf{R}_R(z, \cdot) * \boldsymbol{E}^{-}(z, \cdot)(s) \\
&\boldsymbol{E}^{-}(0, s + z/v) = \mathbf{Q}^{-}(z, 0) \left\{ \boldsymbol{E}^{-}(z, s) + \mathbf{T}_R(z, \cdot) * \boldsymbol{E}^{-}(z, \cdot)(s) \right\}
\end{aligned}
\tag{6.1}
$$

The kernels are defined in the region $z \in (0, d)$ and $s > 0$. Due to causality, all scattering kernels are identically zero for $s < 0$. In the definitions of the transmission operators the $\boldsymbol{Q}^{\pm}$ matrices describe right and left going wave fronts propagating through the subslab at velocity v, see Equation (5.1). The physical scattering kernels, corresponding to the scattering operators for the physical slab $[0, d]$, are $\mathbf{R}_L(0, s)$, $\mathbf{T}_L(0, s)$, $\mathbf{R}_R(d, s)$ and $\mathbf{T}_R(d, s)$.

Combined use of the definitions above and Equation (3.1) result in the imbedding equations (see Refs [8, 12]).

$$(v\partial_z - 2\partial_s)\mathbf{R}_L = \partial_s\boldsymbol{\Delta}_{21} + \partial_s\{\boldsymbol{\Delta}_{22} * \mathbf{R}_L - \mathbf{R}_L * \boldsymbol{\Delta}_{11} - \mathbf{R}_L * \boldsymbol{\Delta}_{12} * \mathbf{R}_L\}$$
$$v\partial_z\mathbf{T}_L = -\partial_s\boldsymbol{\Delta}_{11} - v\mathbf{a}^+\mathbf{T}_L - \partial_s\{(\mathbf{I} + \mathbf{T}_L*)\boldsymbol{\Delta}_{12} * \mathbf{R}_L + \mathbf{T}_L * \boldsymbol{\Delta}_{11}\}$$
$$(v\partial_z + 2\partial_s)\mathbf{R}_R = \partial_s\boldsymbol{\Delta}_{12} + \partial_s\{\boldsymbol{\Delta}_{11} * \mathbf{R}_R - \mathbf{R}_R * \boldsymbol{\Delta}_{22} - \mathbf{R}_R * \boldsymbol{\Delta}_{21} * \mathbf{R}_R\}$$
$$v\partial_z\mathbf{T}_R = -\partial_s\boldsymbol{\Delta}_{22} - v\mathbf{a}^-\mathbf{T}_R - \partial_s\{(\mathbf{I} + \mathbf{T}_R*)\boldsymbol{\Delta}_{21} * \mathbf{R}_R + \mathbf{T}_R * \boldsymbol{\Delta}_{22}\}$$

$$(6.2)$$

The initial values are

$$\mathbf{R}_L(z, 0^+) = -\frac{1}{2}\boldsymbol{\Delta}_{21}(z, 0^+)$$

$$\mathbf{T}_L(z, 0^+) = \frac{1}{v}\int_z^d \mathbf{Q}^+(z', z)\Big\{\partial_s\boldsymbol{\Delta}_{11}(z', 0^+)$$
$$- \frac{1}{2}\boldsymbol{\Delta}_{12}(z', 0^+)\boldsymbol{\Delta}_{21}(z', 0^+)\Big\}\mathbf{Q}^+(z, z')\,dz'$$

$$\mathbf{R}_R(z, 0^+) = \frac{1}{2}\boldsymbol{\Delta}_{12}(z, 0^+)$$

$$\mathbf{T}_R(z, 0^+) = \frac{1}{v}\int_0^z \mathbf{Q}^-(z', z)\Big\{-\partial_s\boldsymbol{\Delta}_{22}(z', 0^+)$$
$$- \frac{1}{2}\boldsymbol{\Delta}_{21}(z', 0^+)\boldsymbol{\Delta}_{12}(z', 0^+)\Big\}\mathbf{Q}^-(z, z')\,dz'$$

For the reflection kernels finite jump discontinuities appear along the characteristics $s = 2(d - z)/v$ and $s = 2z/v$. They are

$$[\mathbf{R}_L(z, 2(d - z)/v)]_-^+ = \frac{1}{2}\mathbf{Q}^-(d, z)\boldsymbol{\Delta}_{21}(d, 0^+)\mathbf{Q}^+(z, d)$$

$$[\mathbf{R}_R(z, 2z/v)]_-^+ = -\frac{1}{2}\mathbf{Q}^+(0, z)\boldsymbol{\Delta}_{12}(0, 0^+)\mathbf{Q}^-(z, 0)$$

and the boundary values, corresponding to no scattering when the slab vanishes, are

$$\mathbf{R}_L(d, s) = \mathbf{0}$$
$$\mathbf{T}_L(d, s) = \mathbf{0}$$
$$\mathbf{R}_R(0, s) = \mathbf{0}$$
$$\mathbf{T}_R(0, s) = \mathbf{0}$$

6.2   The Green functions method

An analogous set of equations can be derived using matrix-valued Green functions. In the Green functions method, the external incident fields $\boldsymbol{E}^+(0, s)$ or $\boldsymbol{E}^-(d, s)$, for incidence from the left and from the right, respectively, are mapped to the split internal fields $\boldsymbol{E}^\pm(z, s)$ in the slab (see Ref. [11]). The 2×2 matrix-valued Green functions, $\boldsymbol{G}_L^\pm(z, s)$ and $\boldsymbol{G}_R^\pm(z, s)$, are defined by

$$\boldsymbol{E}^+(z, s + z/v) = \mathbf{Q}^+(0, z)\boldsymbol{E}^+(0, s) + \mathbf{G}_L^+(z, \cdot) * \mathbf{Q}^+(0, z)\boldsymbol{E}^+(0, \cdot)(s)$$
$$\boldsymbol{E}^-(z, s + z/v) = \mathbf{G}_L^-(z, \cdot) * \mathbf{Q}^+(0, z)\boldsymbol{E}^+(0, \cdot)(s)$$
$$\boldsymbol{E}^+(z, s + (d - z)/v) = \mathbf{G}_R^+(z, \cdot) * \mathbf{Q}^-(d, z)\boldsymbol{E}^-(d, \cdot)(s)$$
$$\boldsymbol{E}^-(z, s + (d - z)/v) = \mathbf{Q}^-(d, z)\boldsymbol{E}^-(d, s) + \mathbf{G}_R^-(z, \cdot) * \mathbf{Q}^-(d, z)\boldsymbol{E}^-(d, \cdot)(s)$$

(6.3)

The Green functions are defined in the domain $z \in (0, d)$ and $s > 0$. Due to causality, all the Green functions vanish identically for $s < 0$. In these definitions the incident fields are first propagated, by the wave front matrices $\mathbf{Q}^\pm$ see (5.1), to the coordinate z inside the slab. From (3.1) and the definitions above, the Green functions equations are derived. The result is (cf. Ref. [8])

$$v\partial_z \mathbf{G}_L^+ = \mathbf{G}_L^+ v\mathbf{a}^+ + \partial_s \left\{ \boldsymbol{\Delta}_{11} + \boldsymbol{\Delta}_{11} * \mathbf{G}_L^+ + \boldsymbol{\Delta}_{12} * \mathbf{G}_L^- \right\}$$
$$(v\partial_z - 2\partial_s)\mathbf{G}_L^- = \mathbf{G}_L^- v\mathbf{a}^+ + \partial_s \left\{ \boldsymbol{\Delta}_{21} + \boldsymbol{\Delta}_{21} * \mathbf{G}_L^+ + \boldsymbol{\Delta}_{22} * \mathbf{G}_L^- \right\}$$
$$(v\partial_z + 2\partial_s)\mathbf{G}_R^+ = \mathbf{G}_R^+ v\mathbf{a}^- + \partial_s \left\{ \boldsymbol{\Delta}_{12} + \boldsymbol{\Delta}_{11} * \mathbf{G}_R^+ + \boldsymbol{\Delta}_{12} * \mathbf{G}_R^- \right\}$$
$$v\partial_z \mathbf{G}_R^- = \mathbf{G}_R^- v\mathbf{a}^- + \partial_s \left\{ \boldsymbol{\Delta}_{22} + \boldsymbol{\Delta}_{21} * \mathbf{G}_R^+ + \boldsymbol{\Delta}_{22} * \mathbf{G}_R^- \right\}$$

The initial values are

$$\mathbf{G}_L^-(z, 0^+) = -\frac{1}{2}\boldsymbol{\Delta}_{21}(z, 0^+)$$

$$\mathbf{G}_L^+(z, 0^+) = \frac{1}{v} \int_0^z \mathbf{Q}^+(z', z) \Big\{ \partial_s \boldsymbol{\Delta}_{11}(z', 0^+)$$
$$- \frac{1}{2}\boldsymbol{\Delta}_{12}(z', 0^+)\boldsymbol{\Delta}_{21}(z', 0^+) \Big\} \mathbf{Q}^+(z, z') \, dz'$$

$$\mathbf{G}_R^+(z, 0^+) = \frac{1}{2}\boldsymbol{\Delta}_{12}(z, 0^+)$$

$$\mathbf{G}_R^-(z, 0^+) = \frac{1}{v} \int_z^d \mathbf{Q}^-(z', z) \Big\{ -\partial_s \boldsymbol{\Delta}_{22}(z', 0^+)$$
$$- \frac{1}{2}\boldsymbol{\Delta}_{21}(z', 0^+)\boldsymbol{\Delta}_{12}(z', 0^+) \Big\} \mathbf{Q}^-(z, z') \, dz'$$

Reflected fields are generated by $\mathbf{G}_L^-$ and $\mathbf{G}_R^+$ (cf. imbedding reflection kernels) and for these Green functions jump discontinuities appear along $s = 2(d - z)/v$ and $s = 2z/v$. They are

$$\left[\mathbf{G}_L^-(z, 2(d - z)/v) \right]_-^+ = \frac{1}{2}\mathbf{Q}^-(d, z)\boldsymbol{\Delta}_{21}(d, 0^+)\mathbf{Q}^+(z, d)$$

$$\left[\mathbf{G}_R^+(z, 2z/v) \right]_-^+ = -\frac{1}{2}\mathbf{Q}^+(0, z)\boldsymbol{\Delta}_{12}(0, 0^+)\mathbf{Q}^-(z, 0)$$

In consistency with the definitions of the Green functions, the boundary values are

$$\mathbf{G}_L^+(0,s) = \mathbf{0}$$
$$\mathbf{G}_L^-(d,s) = \mathbf{0}$$
$$\mathbf{G}_R^+(0,s) = \mathbf{0}$$
$$\mathbf{G}_R^-(d,s) = \mathbf{0}$$

(6.4)

6.3 Relations between scattering kernels

The imbedding kernels defined in (6.1) are related to the Green functions defined in (6.3). These relations can be found by combined use of the definitions (6.1) and (6.3). The result is

$$\mathbf{G}_L^-(z,s) = \mathbf{R}_L(z,s) + \mathbf{R}_L(z,\cdot) * \mathbf{G}_L^+(z,\cdot)(s)$$
$$\mathbf{Q}^+(d,z)\mathbf{G}_L^+(d,s)\mathbf{Q}^+(z,d) = \mathbf{G}_L^+(z,s) + \mathbf{T}_L(z,s) + \mathbf{T}_L(z,\cdot) * \mathbf{G}_L^+(z,\cdot)(s)$$
$$\mathbf{G}_R^+(z,s) = \mathbf{R}_R(z,s) + \mathbf{R}_R(z,\cdot) * \mathbf{G}_R^-(z,\cdot)(s)$$
$$\mathbf{Q}^-(0,z)\mathbf{G}_R^-(0,s)\mathbf{Q}^-(z,0) = \mathbf{G}_R^-(z,s) + \mathbf{T}_R(z,s) + \mathbf{T}_R(z,\cdot) * \mathbf{G}_R^-(z,\cdot)(s)$$

Specifically, let $z = 0$ and $z = d$ in these equations. The boundary values corresponding to the physical slab $[0,d]$ are then derived using (6.4).

$$\mathbf{G}_L^-(0,s) = \mathbf{R}_L(0,s)$$
$$\mathbf{G}_L^+(d,s) = \mathbf{Q}^+(0,d)\mathbf{T}_L(0,s)\mathbf{Q}^+(d,0)$$
$$\mathbf{G}_R^+(d,s) = \mathbf{R}_R(d,s)$$
$$\mathbf{G}_R^-(0,s) = \mathbf{Q}^-(d,0)\mathbf{T}_R(d,s)\mathbf{Q}^-(0,d)$$

7 Mirror image invariance

The equations for scattering from the left ($\hat{k} = \hat{k}^+$) are connected to the equations for the mirror image situation ($\hat{k} = \hat{k}^-$). To see the connection, a spatial reflection in the plane $z = d/2$ is performed

$$\begin{cases} z \to d - z \\ \mathbf{\Delta}_L(z,s) \to \mathbf{\Delta}_R(d-z,s) \\ \pm \to \mp \\ L \to R \end{cases}$$

(7.1)

Here

$$\mathbf{\Delta}_L(z,s) = \begin{pmatrix} \mathbf{\Delta}_{11}(z,s) & \mathbf{\Delta}_{12}(z,s) \\ \mathbf{\Delta}_{21}(z,s) & \mathbf{\Delta}_{22}(z,s) \end{pmatrix}$$

$$\mathbf{\Delta}_R(z,s) = -\begin{pmatrix} \mathbf{\Delta}_{22}(z,s) & \mathbf{\Delta}_{21}(z,s) \\ \mathbf{\Delta}_{12}(z,s) & \mathbf{\Delta}_{11}(z,s) \end{pmatrix}$$

The scattering kernels are determined by the $\mathbf{\Delta}_{kl}$ matrices which in turn are determined by the medium. If this dependence is written out explicitly the mirror image transformation (7.1) states

$$\mathbf{R}_L(z,s) = \mathcal{R}\left[\mathbf{\Delta}_L(z,s)\right]$$
$$\mathbf{R}_R(d-z,s) = \mathcal{R}\left[\mathbf{\Delta}_R(d-z,s)\right]$$
$$\mathbf{T}_L(z,s) = \mathcal{T}\left[\mathbf{\Delta}_L(z,s)\right]$$
$$\mathbf{T}_R(d-z,s) = \mathcal{T}\left[\mathbf{\Delta}_R(d-z,s)\right]$$
$$\mathbf{G}_L^+(z,s) = \mathcal{G}_\infty\left[\mathbf{\Delta}_L(z,s)\right]$$
$$\mathbf{G}_R^-(d-z,s) = \mathcal{G}_\infty\left[\mathbf{\Delta}_R(d-z,s)\right]$$
$$\mathbf{G}_L^-(z,s) = \mathcal{G}_\in\left[\mathbf{\Delta}_L(z,s)\right]$$
$$\mathbf{G}_R^+(d-z,s) = \mathcal{G}_\in\left[\mathbf{\Delta}_R(d-z,s)\right]$$

where $\mathcal{R}$, $\mathcal{T}$, $\mathcal{G}_\infty$ and $\mathcal{G}_\in$ are the fundamental maps of the direct problem. Hence, in the imbedding case there are only two different fundamental maps $\mathcal{R}$ and $\mathcal{T}$ with two different inputs resulting in four different scattering kernels $\mathbf{R}_{L,R}$ and $\mathbf{T}_{L,R}$. If $\mathbf{\Delta}_L(z,s) = \mathbf{\Delta}_R(d-z,s)$ then the scattering kernels for scattering from the right are just mirror images (with respect to the symmetry plane $z = \frac{d}{2}$) of the scattering kernels for scattering from the left. Hence, in this case, the mirror image scattering experiment gives no new information about the medium.

To find conditions for mirror image invariant homogeneous media it is relevant to study $\mathbf{\Delta}_L(s) = \mathbf{\Delta}_R(s)$ which implies $\mathbf{\Delta}_{11} = -\mathbf{\Delta}_{22}$ and $\mathbf{\Delta}_{12} = -\mathbf{\Delta}_{21}$. Equation (3.2) then implies that $\mathbf{\Delta}_{ee,mm}$ are both zero. If this is the case the medium is mirror image invariant for any angle of incidence. Due to the unique solubility of the resolvent equation (2.4), the result, in terms of the susceptibility matrix components, is

$$\chi_{31}(t) \equiv \chi_{32}(t) \equiv \chi_{13}(t) \equiv \chi_{23}(t) \equiv 0$$

For normal incidence any homogeneous anisotropic medium, of the class treated in this paper, is mirror image invariant. This is so since $\boldsymbol{k}_\parallel = \mathbf{0}$ implies $\mathbf{\Delta}_{ee} \equiv \mathbf{\Delta}_{mm} \equiv \mathbf{\Delta}_{em} \equiv \mathbf{0}$.

The above analysis leads to a class of media with mirror image invariant scattering properties. This class is exactly the same as the class of media with mirror image invariant susceptibility dyadics. To see this, it is relevant to study the components $\overline{\overline{\chi}}_\parallel$, $\boldsymbol{a}$, $\boldsymbol{b}$ and c of the decomposition (2.1) under the transformation $\hat{n} \to -\hat{n}$. Equation (2.2) implies that the image (the components in the decomposition) of the susceptibility dyadic $\overline{\overline{\chi}}$ is invariant only if both $\boldsymbol{a}$ and $\boldsymbol{b}$ are zero. Equation (3.3) then implies the above result ($\overline{\overline{\Delta}}_{ee} \equiv \overline{\overline{\Delta}}_{mm} \equiv \overline{\overline{0}}$).

8 The inverse scattering problem

The physical scattering kernels for a mirror image invariant homogeneous medium satisfy

$$\mathbf{R}_L(0, s) = \mathbf{R}_R(d, s)$$
$$\mathbf{T}_L(0, s) = \mathbf{T}_R(d, s)$$

Thus, incident fields from the right give no new information about the medium. The inverse scattering problem is to reconstruct the five susceptibility kernels $\chi_{11}(s)$, $\chi_{12}(s)$, $\chi_{21}(s)$, $\chi_{22}(s)$ and $\chi_{33}(s)$. This can be done from either reflection and transmission data at oblique incidence or from reflection data from two experiments (one at normal incidence and one at oblique incidence). The latter case has the advantage that it is enough to make measurements on one side of the slab. Hence, in the following only scattering from the left is considered and therefore the L- and R-indices are not written out.

For the first round trip ($vs < 2d$) the equations become particularly simple. Due to causality, the scattering effects from the right boundary $z = d$ can not influence the reflection data at $z = 0$ and the imbedding equation for the reflection kernel becomes z independent. An integration with respect to time of the remaining terms yields

$$2\mathbf{R} + \mathbf{\Delta}^+ + \mathbf{\Delta}^- * \mathbf{R} + \mathbf{R} * \mathbf{\Delta}^- + \mathbf{R} * \mathbf{\Delta}^+ * \mathbf{R} = \mathbf{0} \tag{8.1}$$

where $\mathbf{\Delta}^\pm = \mathbf{\Delta}_{me} \pm \mathbf{\Delta}_{em}$. For normal incidence $\mathbf{\Delta}_{em} \equiv \mathbf{0}$ which yields (cf. Ref. [8])

$$2\mathbf{R} + \mathbf{\Delta}_{me} + \mathbf{\Delta}_{me} * \mathbf{R} + \mathbf{R} * \mathbf{\Delta}_{me} + \mathbf{R} * \mathbf{\Delta}_{me} * \mathbf{R} = \mathbf{0} \tag{8.2}$$

This is a system of Volterra equations of the second kind in $\mathbf{\Delta}_{me}$ and hence the inverse problem is well posed. Solution of this equation yields the kernels $\chi_{11}(s)$, $\chi_{12}(s)$, $\chi_{21}(s)$ and $\chi_{22}(s)$. The remaining kernel $\chi_{33}(s)$ may then be reconstructed from a scattering experiment at oblique incidence. Inserting the known susceptibility kernels in (8.1) and taking the 22-component a linear Volterra equation of the second kind for the resolvent L is obtained.

$$f - 2R_{22} * f + R_{22} * f * R_{22} + 2R_{22} + g_{22}$$
$$+ g_{2i} * R_{i2} + R_{2i} * g_{i2} + R_{2i} * g_{ij} * R_{j2} = 0$$
$$f = \frac{1}{2} \left| \frac{k_\parallel}{k_n} \right|^2 L = \mathbf{\Delta}_{em,22}$$
$$g_{ij} = \mathbf{\Delta}_{me,ij}$$

Here summation over repeated indices is understood. This is again a well posed problem which determines the resolvent L. The resolvent equation (2.4) then finally gives χ_{33} for times less than one round trip ($s \in [0, 2d/v]$).
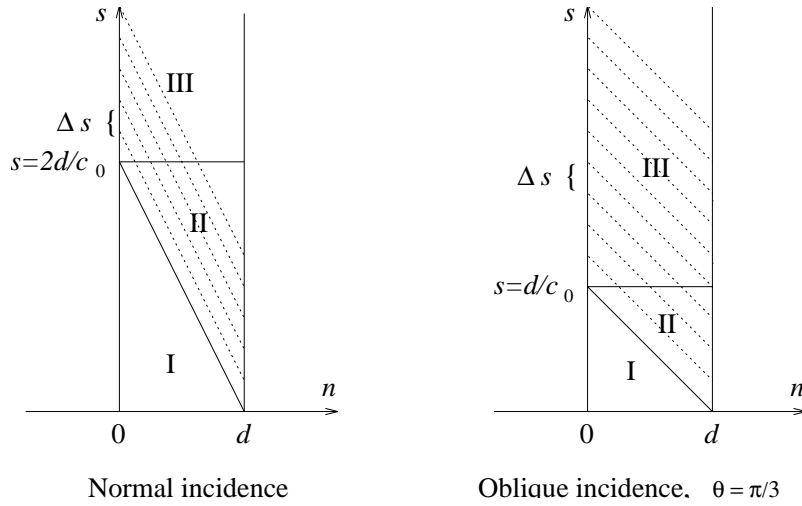
Figure 3: The scattering problem in the zs-plane for normal and oblique incidence. Diagonal lines indicate the characteristics of the equations for the reflection kernels.

The other components of (8.1) give three Volterra equations of the first kind in the resolvent L. Therefore, these equations are less suitable for the inverse scattering problem. Since the resolvent is obtained from the 22-component equation, these equations are in fact three constraints on the reflection kernels R_{ij} at oblique incidence. Hence there are $8 - 3 = 5$ degrees of freedom which is one for each of the unknown susceptibility kernels.

For times greater than the first round trip, the effect of the back edge $z = d$ of the slab cannot be neglected and thence the z-derivatives in the imbedding equation must be regarded. At a general oblique incidence this yields an integrodifferential equation for the two matrices $\mathbf{\Delta}^{\pm}$ and at normal incidence a similar equation with only $\mathbf{\Delta}_{me}$ is obtained, see (6.2). From normal incidence reflection data, the matrix $\mathbf{\Delta}_{me}$ can be reconstructed and thus $\chi_{\parallel}$ is easily obtained. This is then transformed to $\mathbf{\Delta}_{me}$ for a given oblique incidence. Using these data and reflection data from the oblique incidence experiment, the 22-component of $\mathbf{\Delta}_{em}$ matrix is obtained. Finally χ_{33} can be calculated by use of the resolvent equation (2.4).

8.1 Algorithm and numerical implementation

The total inversion algorithm uses the scattering data $\mathbf{R}(0; 0, s)$ and $\mathbf{R}(\theta; 0, s)$ corresponding to a normal and an oblique incidence experiment. An additional argument θ is introduced to distinguish reflection data at different angle of incidence. The algorithm is:

1: Normal incidence data $\mathbf{R}(0; 0, s)$.

a) Reconstruct $\mathbf{\Delta}_{me}(0; s)$ for the first round trip $s \in [0, 2d/c_0]$ using (8.2).

b) Propagate $\mathbf{R}(0; 0, s)$ into region I. Use $\mathbf{R}(0; 0, 0)$ to calculate the finite jump

discontinuity along the characteristic $s = 2(d-z)/c_0$ (solid diagonal line in Fig. 3) and then calculate $\mathbf{R}(0; z, (2(d-z)/c_0)^+)$. Differentiate $\boldsymbol{\Delta}_{me}(0; s)$ and use $\partial_s \boldsymbol{\Delta}_{me}(0; s)$ and $\boldsymbol{\Delta}_{me}(0; 0)$ in region I+II.

c) Time-step j (starting with $j = 1$). Integrate the imbedding equation along the characteristic $s = 2(d-z)/c_0 + j\Delta s$ (dotted line in Fig. 3) in region II+III. The boundary value at $z = d$ is used to generate $\mathbf{R}(0; z, s)$ on the characteristic inside the slab where $\partial_s \boldsymbol{\Delta}_{me}(s)$ is known. At the left endpoint $z = 0$, $s = 2d/c_0 + j\Delta s$ the reflection data $\mathbf{R}(0; 0, 2d/c_0 + j\Delta s)$ is known and $\partial_s \boldsymbol{\Delta}_{me}(0; 2d/c_0 + j\Delta s)$ can be calculated. Propagate $\partial_s \boldsymbol{\Delta}_{me}(0; 2d/c_0 + j\Delta s)$ into region III and repeat step c) with $j \to j + 1$.

d) Reconstruct $\boldsymbol{\Delta}_{me}(0; s)$ in region III by integrating $\partial_s \boldsymbol{\Delta}_{me}(0; s)$.

2: Oblique incidence data $\mathbf{R}(\theta; 0, s)$.

**a)** Transform $\boldsymbol{\Delta}_{me}(0; s)$ to fit oblique incidence

$$\boldsymbol{\Delta}_{me}(\theta; s) = \frac{1}{\cos\theta}\boldsymbol{\Gamma}(\theta)\boldsymbol{\Delta}_{me}(0; s)$$

b) Use $\boldsymbol{\Delta}_{me}(\theta; s)$ and $\mathbf{R}(\theta; 0, s)$ to reconstruct the 22-component of $\boldsymbol{\Delta}_{em}(\theta; s)$ following steps analogous to 1:a-d above. Inside the slab, all four components of the PDE are used to calculate $\mathbf{R}(\theta; z, s)$ while at the left endpoint where $\boldsymbol{\Delta}_{em}(s)$ is calculated only the 22-component is used. This gives the resolvent $L(s)$.

c) Solve the resolvent equation (2.4) to get $\chi_{33}(s)$. This closes the algorithm.

The PDE's are discretized using the trapezoidal rule for integrals. In region II+III each PDE consists of two parts, see Eq. (6.2). The left hand side of (6.2) is a total derivative along a characteristic and the right hand side is a total time-derivative. In the above algorithm the right hand side is implemented by performing a differentiation with respect to time and an integration along the characteristic. This yields an equation in $\Delta^{\pm}(0)$ and the time-derivatives $\partial_s \Delta^{\pm}(s)$. In region I Eq. (8.1) holds and $\Delta^{\pm}(s)$ are obtained directly. Therefore, the step from region I into region II require numerical differentiation (a three point formula has been implemented).

To avoid numerical differentiation, a different method including an additional integration of the PDE's along time s has also been implemented. However, this trick introduces severe instabilities at other steps in the algorithm and in a comparison between the methods the former one is much more stable. The numerical examples presented in Section 9 use this former method.
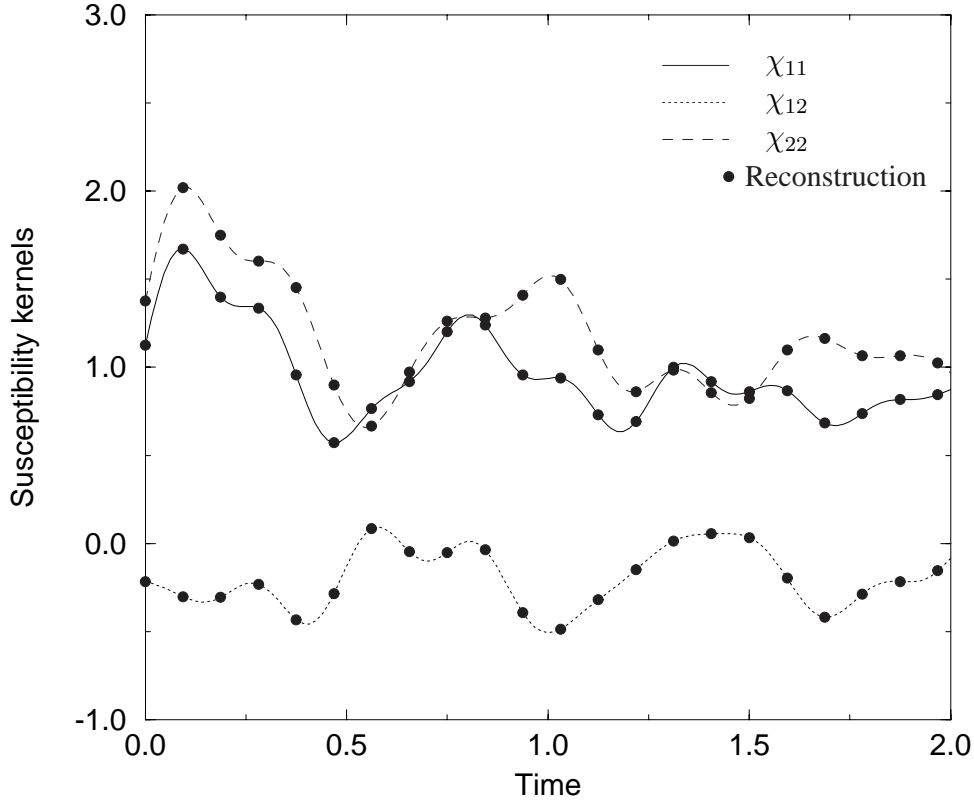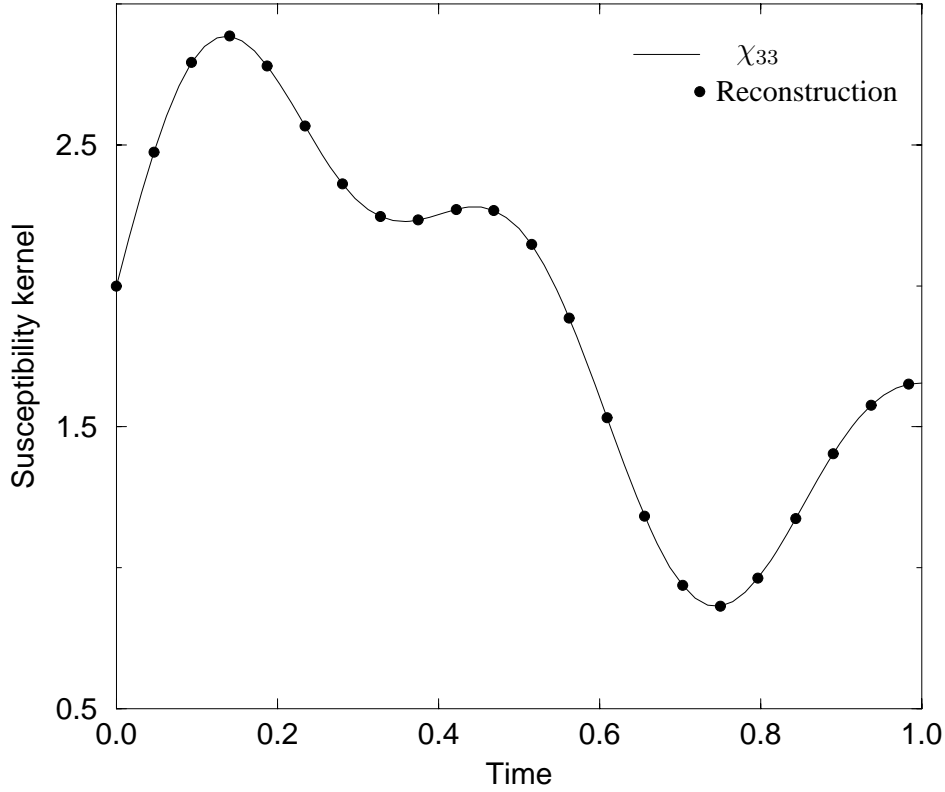
Figure 4: Reconstructions of the components of $\boldsymbol{\chi}_{\parallel}$ in Example 1. The time scale is given in units of d/c_0 and the vertical axis in units of c_0/d.

9   Numerical examples

In this section some numerical examples that illustrate the analysis are presented. Only homogeneous mirror image invariant media are considered. This is a rather wide class of media. However, the orientation of the symmetry axes of the medium restricts the class. For a biaxial medium one of the optical axes must be along the z-axis and the other one must lie in the xy-plane (see Ref. [3]). Another class of mirror image invariant media are the gyrotropic media with an external magnetic induction along the z-axis, see Refs [4, 18]. The time unit used in this section is $\frac{d}{c_0}$, which correspond to half a round trip at normal incidence, and the frequency unit is $\frac{c_0}{d}$.

Example 1

The first example is a biaxial homogeneous medium with

Figure 5: The reconstruction of χ_{33} in Example 1. The time scale is given in units of d/c_0 and the vertical axis in units of c_0/d.

$$
\boldsymbol{\chi}(t) = \begin{pmatrix} g_1(t)\cos^2\phi + g_2(t)\sin^2\phi & (g_1(t) - g_2(t))\cos\phi\sin\phi & 0 \\ (g_1(t) - g_2(t))\cos\phi\sin\phi & g_1(t)\sin^2\phi + g_2(t)\cos^2\phi & 0 \\ 0 & 0 & g_3(t) \end{pmatrix}
$$

This medium is a diagonal biaxial medium rotated an angle ϕ around the z-axis. Such a medium is the most general mirror image invariant biaxial medium. In this particular example the rotation angle is chosen as $\phi = \frac{\pi}{6}$ and the susceptibility kernels $g_{1,2,3}(t)$ model a Debye-Lorentz material. Specifically, they are

$$
\begin{cases} g_1(t) = e^{-.2t} + .5e^{-.5t}\sin 10t + .2e^{-.5t}\sin 25t \\ g_2(t) = 1.5e^{-.2t} + .7e^{-.5t}\sin 8t + .3e^{-.5t}\sin 20t \\ g_3(t) = 2e^{-.2t} + .9e^{-.5t}\sin 6t + .4e^{-.5t}\sin 15t \end{cases}
$$

This medium is reciprocal since $\chi_{12}(s) = \chi_{21}(s)$. The reconstructions of χ_{11}, χ_{12}, χ_{22} and χ_{33} for the first round trip are depicted in Figures 4 and 5.
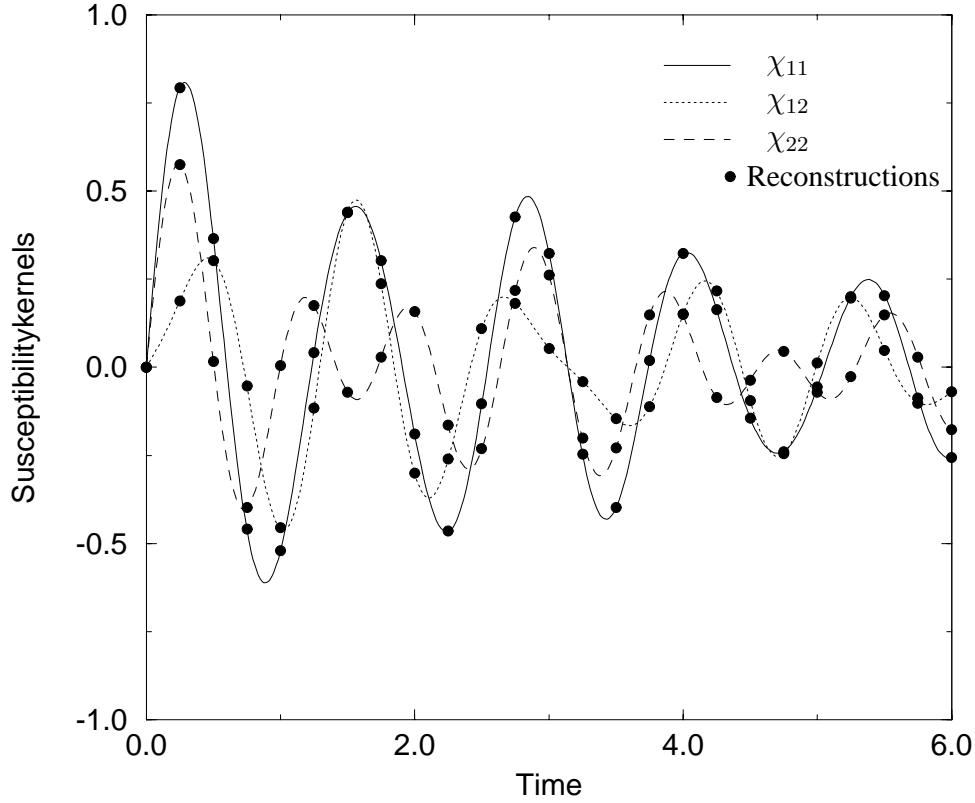
Figure 6: Reconstructions of the components of $\boldsymbol{\chi}_{\parallel}$ in Example 2. Due to reciprocity $\boldsymbol{\chi}_{12} = \boldsymbol{\chi}_{21}$. The time scale is given in units of d/c_0 and the vertical axis in units of c_0/d.
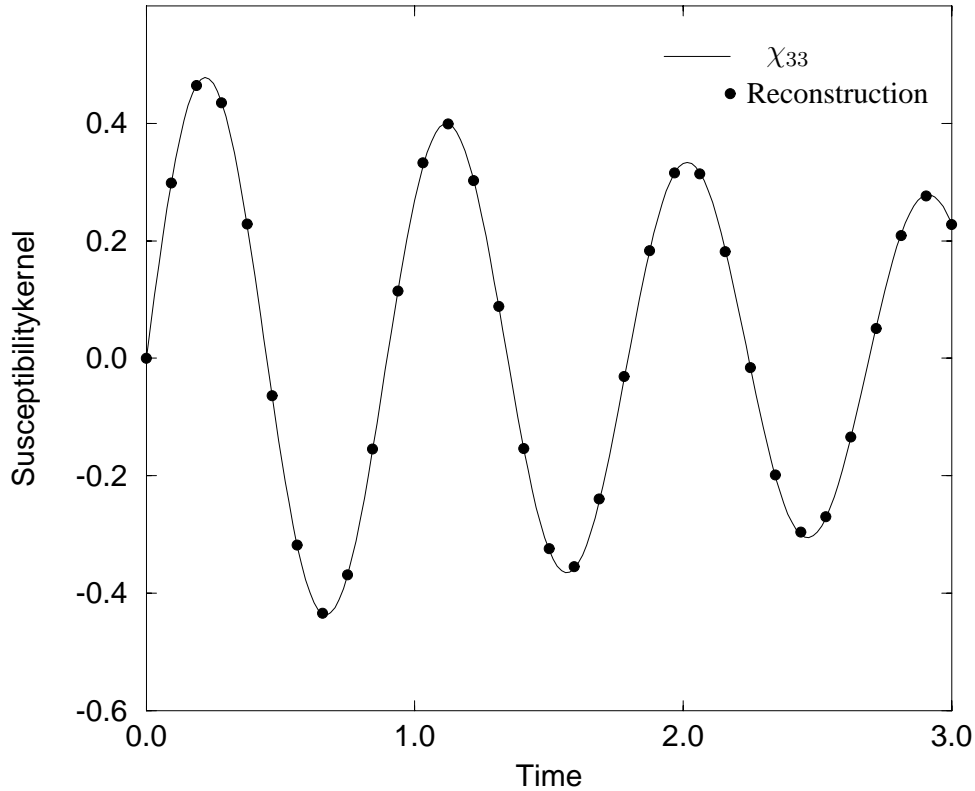
Example 2

In the second example a single mode uniaxial Lorentz medium is illustrated. The susceptibility matrix is

$$\boldsymbol{\chi}(t) = \begin{pmatrix} g_1(t)\cos^2\phi + g(t)\sin^2\phi & (g_1(t) - g(t))\cos\phi\sin\phi & 0 \\ (g_1(t) - g(t))\cos\phi\sin\phi & g_1(t)\sin^2\phi + g(t)\cos^2\phi & 0 \\ 0 & 0 & g(t) \end{pmatrix}$$

and the rotation angle $\phi = \pi/6$. The two susceptibility functions are

$$\begin{cases} g_1(t) = e^{-.2t}\sin 5t \\ g(t) = .5e^{-.2t}\sin 7t \end{cases}$$

In this example the kernels are reconstructed for three round trips. In round trip coordinates (time unit $= d/c_0$) this interval is $[0, 6\cos\theta]$. The reconstruction of $\chi_{33}(s)$ uses oblique incidence data ($\theta = \pi/3$) and is therefore terminated at $s = 3(d/c_0)$. In Figs 6 and 7 reconstructions using clean data are depicted. To

Figure 7: Reconstruction of $\boldsymbol{\chi_{33}}$ in Example 2. The time scale is given in units of d/c_0 and the vertical axis in units of c_0/d.

test the stability of the algorithm the direct scattering data have been corrupted with uniform noise of 3% relative amplitude and then smoothed three times using a five-point formula. Results are depicted in Figs 8 and 9.
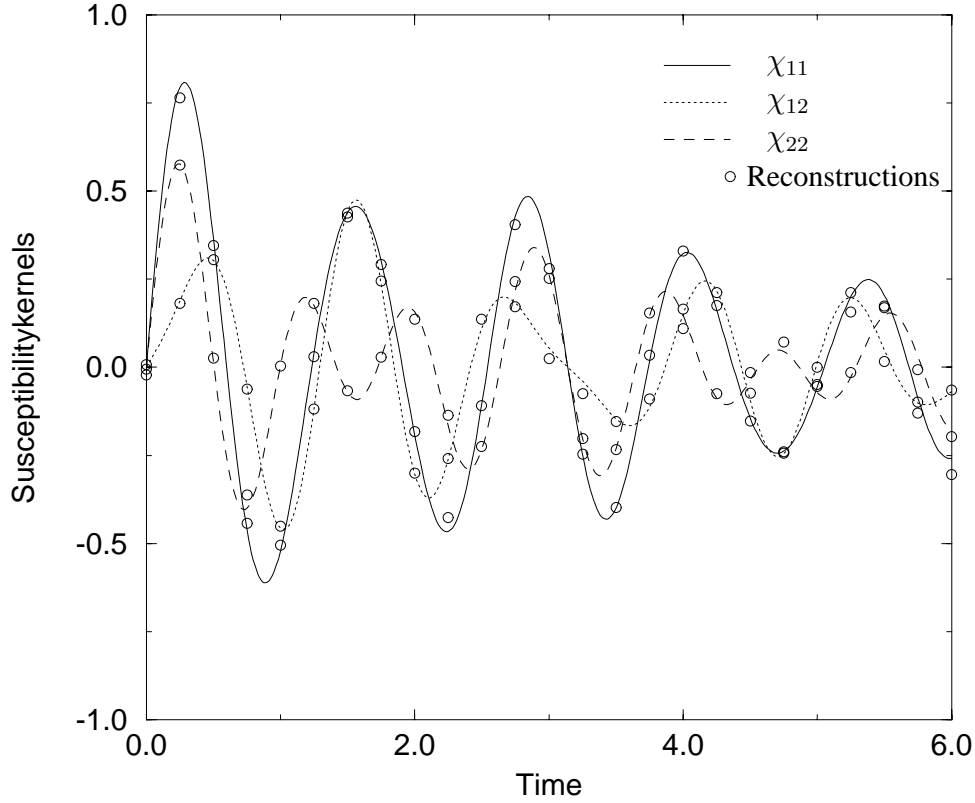
Acknowledgements

References

[1] R. S. Beezley and R. J. Krueger. An electromagnetic inverse problem for dispersive media. *J. Math. Phys.*, **26**(2), 317–325, 1985.

Figure 8: Reconstruction of the components of $\boldsymbol{\chi}_\parallel$ in Example 2 using noisy data. Due to reciprocity $\boldsymbol{\chi}_{12} = \boldsymbol{\chi}_{21}$. The time scale is given in units of d/c_0 and the vertical axis in units of c_0/d.

[2] D. W. Berreman. Optics in stratified and anisotropic media: 4×4 matrix formulation. *J. Opt. Soc. Am.*, **62**, 502–510, 1972.

[3] C. F. Bohren and D. R. Huffman. *Absorption and Scattering of Light by Small Particles*. John Wiley & Sons, New York, 1983.

[4] J. P. Corones, M. E. Davison, and R. J. Krueger. Wave splittings, invariant imbedding and inverse scattering. In A. J. Devaney, editor, *Inverse Optics*, pages 102–106, Bellingham, WA, 1983. Proc. SPIE 413, SPIE.

[5] J. P. Corones, G. Kristensson, P. Nelson, and D. L. Seth, editors. *Invariant Imbedding and Inverse Problems*. SIAM, Philadelphia, 1992.

[6] K. Eidner. Light propagation in stratified anisotropic media: Orthogonality and symmetry of the 4×4 matrix formalisms. *J. Opt. Soc. Am. A*, **6**(11), 1657–1660, 1989.
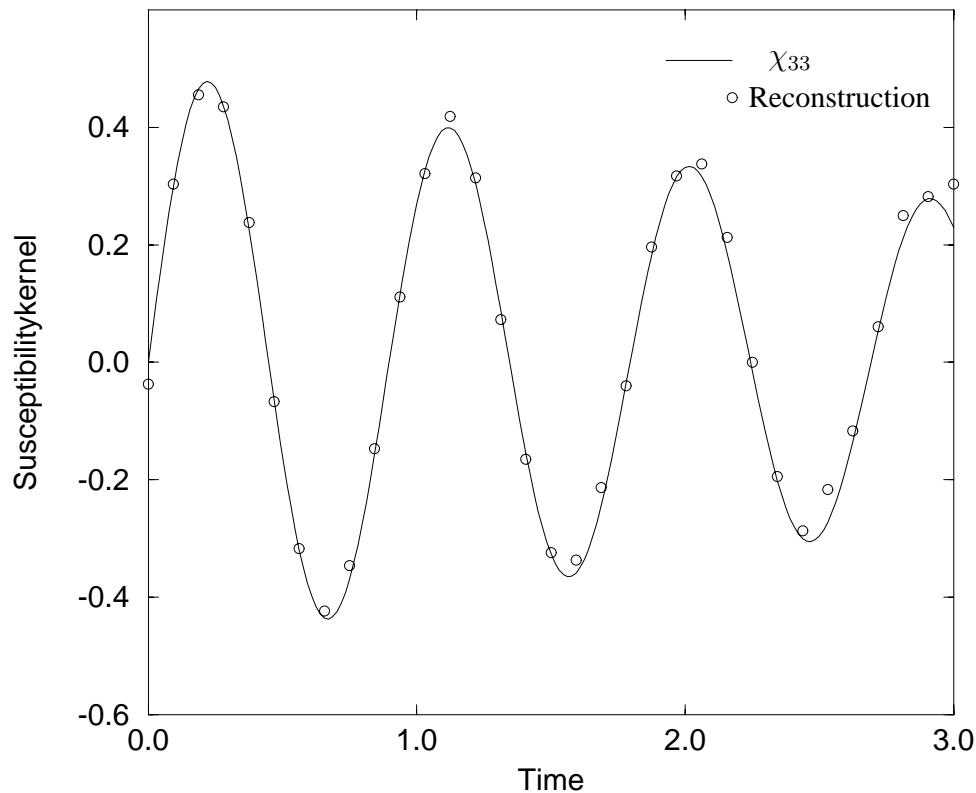
Figure 9: Reconstruction of $\boldsymbol{\chi}_{33}$ in Example 2 using noisy data. The time scale is given in units of d/c_0 and the vertical axis in units of c_0/d.

[7] M. Foresti. Plane-wave propagation in a plane-oriented nematic liquid-crystal multilayer: The case of a wave incident upon the plane containing the liquid-crystal directors. *J. Opt. Soc. Am. A*, **6**(9), 1254–1259, 1989.

[8] J. Fridén, G. Kristensson, and R. D. Stewart. Transient electromagnetic wave propagation in anisotropic dispersive media. *J. Opt. Soc. Am. A*, **10**(12), 2618–2627, 1993.

[9] A. Karlsson and G. Kristensson. Constitutive relations, dissipation and reciprocity for the Maxwell equations in the time domain. *J. Electro. Waves Applic.*, **6**(5/6), 537–551, 1992.

[10] J. A. Kong. Electromagnetic fields due to dipole antennas over stratified anisotropic media. *Geophysics*, **37**(6), 985–996, 1972.

[11] G. Kristensson. Direct and inverse scattering problems in dispersive media— Green's functions and invariant imbedding techniques. In R. Kleinman, R. Kress, and E. Martensen, editors, *Direct and Inverse Boundary Value Prob-*

lems, Methoden und Verfahren der Mathematischen Physik, Band 37, pages 105–119, Frankfurt am Main, 1991. Peter Lang.

[12] G. Kristensson and R. J. Krueger. Direct and inverse scattering in the time domain for a dissipative wave equation. Part 1: Scattering operators. *J. Math. Phys.*, **27**(6), 1667–1682, 1986.

[13] G. Kristensson and S. Rikte. The inverse scattering problem for a homogeneous bi-isotropic slab using transient data. Technical Report LUTEDX/(TEAT-7022)/1–13/(1992), Lund Institute of Technology, Department of Electromagnetic Theory, P.O. Box 118, S-211 00 Lund, Sweden, 1992.

[14] G. Kristensson and S. Rikte. Transient wave propagation in reciprocal bi-isotropic media at oblique incidence. *J. Math. Phys.*, **34**(4), 1339–1359, 1993.

[15] I. V. Lindell. *Methods for Electromagnetic Field Analysis.* Clarendon Press, Oxford, 1992.

[16] J. C. Monzon. Three-dimensional field representation in a ten-parameter cylindrically symmetric anisotropic material. *IEEE Trans. Antennas Propagat.*, **AP-38**(4), 551–555, 1990.

[17] A. M. Morgan, D. L. Fischer, and E. A. Milne. Electromagnetic scattering by stratified inhomogeneous anisotropic media. *IEEE Trans. Antennas Propagat.*, **AP-35**(2), 191–197, 1987.

[18] H. Otterheim. An inverse scattering problem for gyrotropic media. Technical Report TRITA-TET 93-3, Department of Electromagnetic Theory, S-100 44 Stockholm, Sweden, 1993.

[19] H. Schopper. Zur optik dunner Doppelbrechender und dichroisticher Schichten. *Z. Phys.*, **132**, 146–170, 1952.

[20] O. Schwelb. Stratified lossy anisotropic media: General characteristics. *J. Opt. Soc. Am. A*, **3**(2), 188–193, 1986.

[21] R. D. Stewart. *Transient electromagnetic scattering on anisotropic media.* PhD thesis, Iowa State University, Ames, Iowa, 1989.

[22] S. Teitler and B. W. Henvis. Refraction in stratified, anisotropic media. *J. Opt. Soc. Am.*, **60**, 830–834, 1970.

[23] R. S. Weis and T. K. Gaylord. Electromagnetic transmission and reflection characteristics of anisotropic multilayered structures. *J. Opt. Soc. Am. A*, **4**(9), 1720–1740, 1987.

[24] V. H. Weston. Time-domain wave-splitting of Maxwell's equations. *J. Math. Phys.*, **34**(4), 1370–1392, 1993.

[25] H. Wöhler, G. Fritsch, G. Haas, and D. A. Mlynski. Characteristic matrix method for stratified anisotropic media: Optical properties of special configurations. *J. Opt. Soc. Am. A*, **8**(3), 536–540, 1991.